III International Conference on Particle-based Methods – Fundamentals and Applications
PARTICLES 2013
M. Bischoff, E. Oñate, D.R.J. Owen, E. Ramm & P. Wriggers (Eds)

STUDY OF SPRINGBACK OF GREEN BODIES USING MICROMECHANICAL EXPERIMENTS AND THE DISCRETE ELEMENT METHOD

ERIK OLSSON[1], PER-LENNART LARSSON[1]

[1] Department of Solid Mechanics
Royal Institute of Technology KTH
Teknikringen 8D, SE-100 44 Stockholm, Sweden
e-mail: erolsson@kth.se, pelle@hallf.kth.se

Key words: DEM, Powder Compaction, Spray dried granules, nanoindentation, granule strength measurements

Abstract. The Discrete Element Method (DEM) is today a commonly used tool to simulate compaction of particulate media. The main issue when using DEM in compaction problems is the description of the contact between two powder particles. If the material properties are known, analytical and semi-analytical methods can be used [1, 2] but for many industrial applications, for instance spray dried granules, the mechanical behaviour is unknown.

The compaction behaviour and green properties of a cemented carbide powder is studied in this work and the issue of the contact description is solved by performing experiments on the powder granules. Firstly, compression tests are made on the single granules giving information of the mechanical properties at low strains. To get information at high strains, which are needed in powder compaction simulations, nanoindentation tests are performed. The measured material parameters are used in a FE model of two spheres in contact and the resulting contact law is exported to a DEM program.

The DEM program is used to investigate the compaction properties of a powder compact and especially the springback during unloading which is important for predicting the final shape of the product. The results are compared with presently performed experiments and the applicability range of the discrete element simulations will be discussed.

1 INTRODUCTION

Powder compaction followed by sintering is today a commonly used production route in the industry of hard materials. Due to the influence on the final product from defects formed during the compaction stage, which remains after sintering, there has been an increasing interest in the modelling of powder compaction. This modelling can be performed using a continuum approach relying on constitutive models for porous solids

or using a micromechanical approach where the constitutive behaviour of the individual powder particles is utilized.

The first attempts using a micromechanical model, cf. e.g. [3–5], were based on the assumption of affine motion, i.e. that the motion of each particle is solely given by the macroscopic strain field, and thus not taking particle rearrangement into account. In order to relax this assumption, the Discrete Element Method (DEM) has recently been widely used to simulate compaction of granular materials resulting in a good agreement with compaction experiments [6–8]. In all these micromechanical models, it is essential that the contact force between two powder particles is modelled in an adequate manner to get reliable results. If the constitutive behaviour of the particles is known, solutions for two particles in contact exist for rigid plastic contact behaviour [1] and contacts deforming in a combined elastic-plastic manner [2].

However, for many industrially relevant applications, the constitutive behaviour of the powder particles is not known. One example is cemented carbide granules where small tungsten carbide and cobalt particles ($\sim 1\,\mu$m) are mixed with a polymeric binder and are spray dried to larger granules ($\sim 100\,\mu$m). Therefore, this work is focused on determining the constitutive behaviour of this type of granules which is done by micromechanical experiments. The investigation is restricted to two different cemented carbide powders used in the industry, Powder A and Powder B, with slightly different compaction characteristics. The determined material properties of the powder granules are then used for investigating the compaction behaviour and the elastic springback of the pressed powder compacts.

2 MICROMECHANICAL EXPERIMENTS

In order to determine the unknown constitutive behaviour of the powder granules, two different kinds of micromechanical experiments are performed. In the evaluation of the experiments it is assumed that the constitutive behaviour is governed by classical elastoplasticity following J_2 flow theory with isotropic hardening.

2.1 Granule compression tests

The first kind of experiment performed on the powder granules was a compression test where a single granule is pressed between two rigid plates. A sketch of the test setup is shown in Figure 1. The testing equipment is manufactured by etewe [9].

Prior to testing, the diameters in the x and y direction, D_x and D_y, are measured using an image identification system. The diameter in the z direction, D_z, is then determined as the distance between the plates when the granule starts to take load. For the material characterization, it was thought advisable to only use the most spherical granules. Therefore, a sphericity criterion was defined as

$$\sqrt{(D_x - D)^2 + (D_y - D)^2 + (D_z - D)^2} \leq 2.5\% \tag{1}$$

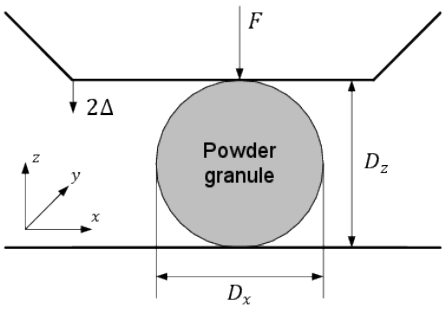

Figure 1: Sketch of the granule compression test setup

where D is the mean diameter $D = (D_x + D_y + D_z)/3$. As a result of this filtering, 9 granules from Powder A and 12 granules from Powder B were included in the analysis. During testing, the force, F, as function of the displacement of the upper plate, Δ, is registered continuously. The outcome of the tests is shown in Figure 2 (a) for Powder A and in Figure 2 (b) for Powder B. Powder A and Powder B are behaving almost the same for displacements $\Delta/R \leq 0.02$, but for higher displacements, Powder B shows a softer behaviour. This could be explained by initiation of micro cracks or that granules of Powder B are less homogenous than the granules of Powder A.

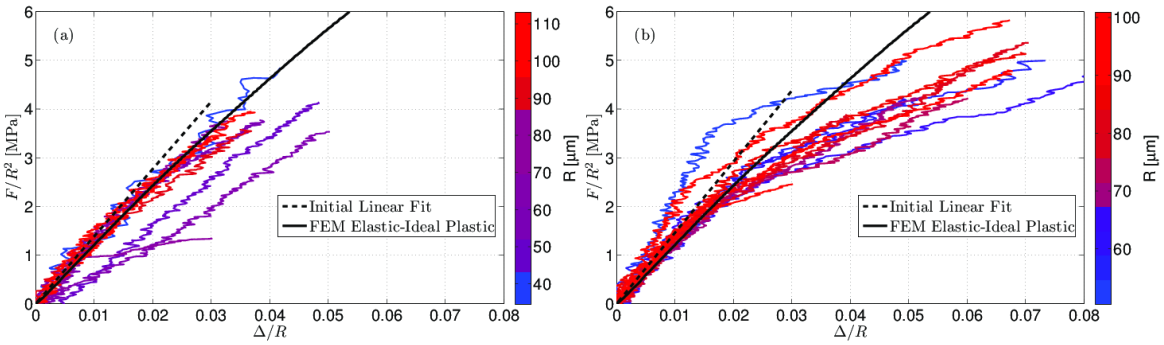

Figure 2: Compression force as function of displacement from the granule compression experiments for (a) Powder A, and (b) Powder B. A linear fit to the initial part of the curves and results from the finite element simulations are also included.

The initial deformation behaviour is close to linear for both granules which, according to the self-similarity solution by Storåkers et. al [1], indicates a ideal-plastic behaviour with negligible elastic deformation. Under such circumstances, the contact force, F, can be written as

$$\frac{F}{R^2} = \alpha \pi c^2 \sigma_Y \frac{\Delta}{R} \tag{2}$$

where α is a parameter taking on the value $\alpha = 5.6$ for two spheres in contact [2], c^2 is an area parameter taking on the value $c^2 = 1.43$ for ideal plastic materials with negligible

elasticity and σ_Y is the yield stress of the spherical particle material. By fitting a linear function to the initial parts of the curves in Figure 2, shown with dashed lines, the yield stress was determined to be $\sigma_Y = 5.8$ MPa for both powders.

However, this analytical solution predicts a too stiff response of the granules for higher deformations. In order to investigate this discrepancy, the granule compression problem was simulated using the Finite Element Method (FEM) and in particular the commercial code ABAQUS [10]. More details of this FE investigation is presented in [11]. The outcome of the FEM analysis is shown in Figure 2 (a) and (b) by solid lines, and they clearly agree better with the experimental results. This discrepancy between the analytical self-similarity solution and the FE simulations can be explained by the effect from large deformations, as shown by Mesarovic and Fleck [12, 13].

In [11], it was also concluded, based on results from FE simulations, that the granules could be considered ideally plastic up to plastic strains of $\varepsilon_H = 0.17$. However, at some value of plastic strain above 0.17, hardening is expected when comparing pertinent compaction results [14, 15] and simulations using ideal-plastic granules.

2.2 Nanoindentation testing

To get information of the constitutive behaviour at high strains, nanoindentation tests were made on the granules. In order to be able to handle the granules during testing, the granules were embedded in epoxy and the surface of the granule-epoxy mixture were afterwards polished to get well-defined indentation imprints. The polished surface with two indentation imprints is shown in Figure 3.

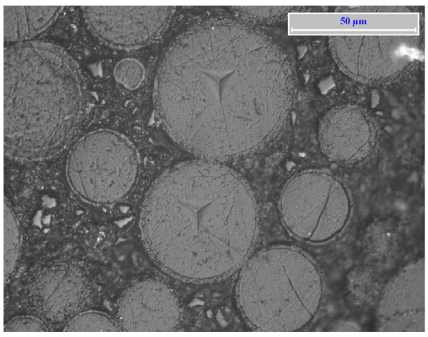

Figure 3: Micrograph of the polished granule-epoxy surface with indentation imprints. The granules are from Powder B.

The nanoindentation tests are performed by pressing a tetrahedral (Berkovic) tip into the tested material, in this case using a controlled load setting. When the indentation depth h has reached 2 µm, the load was held constant for 20 s followed by unloading to 1/5 of the maximum indentation force where the load, again, was held constant, this time for 2 s until continued unloading to zero force. All measured force displacement relations are shown in Figure 4. The plateaus seen in the graphs in Figure 4, when the force is held

constant, indicate a creeping behaviour but this effect will not be considered further in the analysis due to the fact that no established methods exist for taking creeping effects into account in nanoindentation testing and it is deemed that these effects are of minor importance in the present analysis.

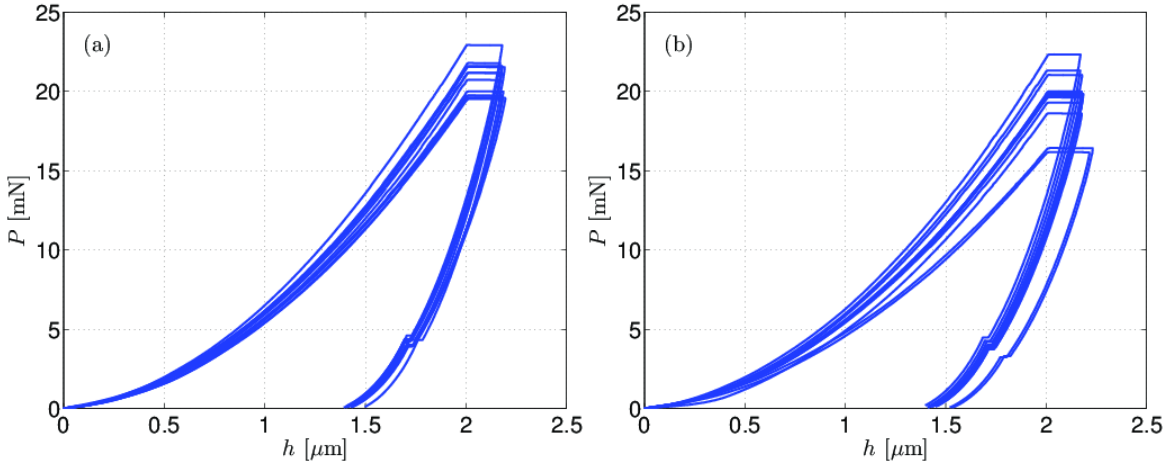

Figure 4: The indentation force P as function of the indentation depth h during the nanoindentation tests. Results for Powder A are presented in (a) and results for Powder B are presented in (b).

The most fundamental property resulting from an indentation test is the indentation hardness defined by $H \equiv P/A_p$ where P is the maximum indentation load and A_p is the projected contact area which is calculated automatically in the testing equipment by carefully calibrating against a material with known hardness. The average hardness values with standard deviations for each powder are presented in Table 1.

The hardness is strongly connected to the plastic behaviour of the material. For a material with regular strain hardening, it is well established that the hardness determined by Berkovic indentation is approximately three times the yield stress at 8 % plastic strain. However, for a material with irregular stress-strain behaviour, as expected here, Larsson [16] discovered that one single stress level is not sufficient to describe the hardness. Instead, a combination of the flow stress at low plastic strain (2 %), $\sigma_{0.02}$, and the flow stress at high plastic strain (35 %), $\sigma_{0.35}$, could be used to calculate the hardness by

$$H = C_1\sigma_{0.02} + C_2\sigma_{0.35} \tag{3}$$

which was determined from extensive FE simulations. Furthermore, the parameters C_1 and C_2 were determined to be $C_1 = C_2 = 1.4$ for a Berkovic indenter. The computed values of the flow stress at 35 % plastic strain, $\sigma_{0.35}$, are included in Table 1 based on the result that $\sigma_{0.02} = \sigma_Y$ as determined by the granule compression tests. Based on the fact that the granules have a constant yield stress for plastic strains $\varepsilon_{pl} \leq 17\%$ and the presently determined flow stresses at $\varepsilon_{pl} = 35\%$, the following constitutive model is

Table 1: Material parameters determined by the micromechanical experiments

Powder	σ_Y [MPa]	H [MPa]	E [GPa]	$\sigma_{0.35}$ [MPa]
Powder A	5.8	234 ± 12	5.72 ± 0.53	161
Powder B	5.8	215 ± 25	5.90 ± 0.69	148

assumed

$$\sigma = \begin{cases} \varepsilon E & \varepsilon E \leq \sigma_Y \\ \sigma_Y & \sigma_Y/E \leq \varepsilon_{pl} \leq \varepsilon_H \\ \sigma_Y + \sigma_0 \left(\varepsilon_{pl} - \varepsilon_H\right)^{1/m} & \varepsilon_{pl} \geq \varepsilon_H \end{cases} \tag{4}$$

To fulfil the determined values of $\sigma_{0.35}$, σ_0 is given by

$$\sigma_0 = \frac{\sigma_{0.35} - \sigma_Y}{(0.35 - \varepsilon_H)^{1/m}} \tag{5}$$

The proposed model contains two unknown parameters to be determined from the compaction experiments described below, the value of the plastic strain at onset of hardening ε_H which lies in the range $0.17 \leq \varepsilon_H \leq 0.35$ and the power-law hardening exponent m.

The unloading section of the force-displacement relations presented in Figure 4 can be used to determine the elastic modulus of the powder particles. If the compliance of the indenter is neglected the elastic modulus can be calculated using the initial unloading stiffness dP/dh by (Oliver and Pharr [17])

$$\frac{E}{1-\nu^2} = \frac{1}{C}\frac{\sqrt{\pi}}{2}\frac{1}{\sqrt{A_p}}\frac{dP}{dh} \tag{6}$$

where the parameter C takes on the value 1.034 for a Berkovic indenter. The value of the Poisson's ratio ν, was assumed to be 0.3. However, in all established formulae for two spheres in contact, the quotient $E/(1-\nu^2)$ appears instead of E alone and thus the results in the sequel should not be dependent on this assumed value of ν.

3 COMPACTION EXPERIMENTS

Compaction experiments were performed using both types of powders in a testing equipment from PTC [18]. Prior to testing, filling densities before and after shaking, D_{bulk} and D_{tap}, and the angle of repose, θ_{rep}, were measured with data reported in Table 2. Powder compacts were pressed uniaxially using a movable upper punch and a fixed lower punch up to different relative densities between $D = 0.45 - 0.60$. The relative density, D, is defined as the density of the in-die compact divided by the sintered density of the final product, reported as D_{th} in Table 2. During compaction, the pressure at the upper and lower punches are registered as well as the position of the upper punch, giving a continuous measurement of the pressure-density response. The in-die dimensions of the

Table 2: Measured powder properties prior to the compaction experiments

Powder	D_{th} [g/cm^3]	D_{bulk} [g/cm^3]	D_{tap} [g/cm^3]	θ_{rep} [$^\circ$]	μ_{part}
Powder A	14.45	3.554	3.8	30	0.58
Powder B	14.64	3.382	3.571	32	0.62

compacts were the same for all experiments; a radius of $R_0 = 6.35$ mm and a height of $L_0 =$10 mm. After ejection, the height, L, and the radius, R, of the cylindrical compacts were measured and the springback in the axial and radial directions were calculated.

4 NUMERICAL SIMULATIONS

The simulations are performed using an in-house developed DEM program. Details of the numerical implementation can be found in [8, 11]. The simulations take both frictional forces and particle rotations into account. The simulations are done with spherical particles of equal radii, R, knowing that the influence of particle size distribution is of minor importance [8].

4.1 Normal contact model

The most critical issue in DEM simulations of powder compaction is the description of the contact forces acting between two contacting powder particles. This description needs to be very accurate to get reliable compaction pressure predictions but also very fast due to the fact that contact forces are evaluated billions of times inone complete simulation. For the contact forces in the normal direction to the contact plane, the contact can be in a loading or an unloading state. When the contact is in the loading state, the contact force as function of indentation depth, $F(h)$, is taken directly from a FE-simulation of two particles in contact using the material model suggested in Section 2.

Unloading of the contact is a more complicated issue due to the fact that the unloading is dependent on the state prior to unloading and not solely a function of the indentation depth. An analytical investigation of this problem was presented in [19] and [2] but the assumed plastic behaviour was assumed to be ideal-plastic and power-law hardening repectively instead of the very irregular stress-strain behaviour determined in Section 2. Here this issue is solved by simulating, using FEM, the unloading of two particles in contact from many different indentation depths ranging from $h/R = 0.02$ to $h/R = 0.6$. The unloading force-displacement sections were then implemented in the DEM code using curve fitting.

It is expected that adhesive bonding between the powder particles could play a major role for the unloading properties of powder compacts as investigated in [20]. Therefore the model for adhesive unloading, presented in [2], is implemented in the DEM code. This model expresses the recovered indentation depth, h_u, and the contact force during unloading, F_u, as function of the radius of the contact area, a. The model relies on the

solution in the absence of adhesion, $h_u^{noAd}(a)$ and $F_u^{noAd}(a)$, respectively and an adhesive term is added derived using linear elastic fracture mechanics arguments leading to

$$F_u = F_u^{noAd}(a) - \sqrt{2GE^*}a^{3/2}\sum_n k_n \frac{2^{5/2+n}\pi^{1/2+n}}{(2+2n)^2-1}\left(\frac{2a}{R}\right)^n \tag{7}$$

$$h_u = h_u^{noAd}(a) + \sqrt{\frac{Ga}{E^*}}\sum_n k_n \frac{2^{2+n}\pi^{n-1/2}}{1+2n}\left(\frac{2a}{R}\right)^n \tag{8}$$

In Eqs. (7)-(8), G is the fracture energy and k_n are parameters to describe the fracture mechanics problem. In [2], the parameters k_n were determined for relatively small indentation depths and thus a new calibration was made by using the same setup and finite element model as in [2] but using deformations up to $h/R = 0.6$ giving $k_0 \equiv 1$, $k_1 = 0.06421$ and $k_2 = 0.0032$. By studying, using FEM the, evolution of the contact area during unloading, the functions $h_u^{noAd}(a)$ and$F_u^{noAd}(a)$ are determined and the adhesive term can be added prior to the inclusion in the DEM code.

4.2 Tangential contact model

An accurate model of the tangential forces (friction) is needed to get accurate predictions. Here, a stick-slip friction model is used assuming that the particles either are in a sticking state with stiffness k_T or in a sliding state modelled by Coulomb friction with coefficient of friction denoted μ. This model can be written mathematically as

$$\boldsymbol{F}_T = \begin{cases} -k_T\boldsymbol{\delta}_t & k_T||\boldsymbol{\delta}_t|| \le \mu F_N \\ -\mu F_N \frac{\boldsymbol{\delta}_t}{||\boldsymbol{\delta}_t||} & k_T||\boldsymbol{\delta}_t|| \ge \mu F_N \end{cases} \tag{9}$$

where $\boldsymbol{\delta}_T$ is the relative displacement of the two particles parallel to the contact plane. For contact between two particles, the coefficient of friction was estimated by use of the angle of repose according to $\mu_{part} = \arctan\theta_{rep}$ giving the values reported in Table 2. For contact between one particle and the die walls a coefficient of friction of $\mu_{wall} = 0.2$ was used based on previous works on pertinent materials [11, 15]. The tangential stiffness for sticking contacts was set to $k_t = 10^4$ N/m which is of the same order of magnitude as the normal stiffness in the granule compression tests.

4.3 Parameter determination

In order to determine the unknown material parameters ε_H and m, as well as the relative density of a powder granule, which is needed when comparing DEM results with experiments, compaction simulations using DEM were performed using a small number of particles ($N = 1000$). By studying when the compact starts to take load and the number of particle contacts increases notably, the relative density of the powder granules were determined to be 0.48 for Powder A and slightly lower för Powder B, 0.46. A parametric study also showed that the value of the power-law exponent should be high, $m \ge 20$, which gives a rapid hardening, and that ε_H is 0.21 for Powder A and 0.23 for Powder B.

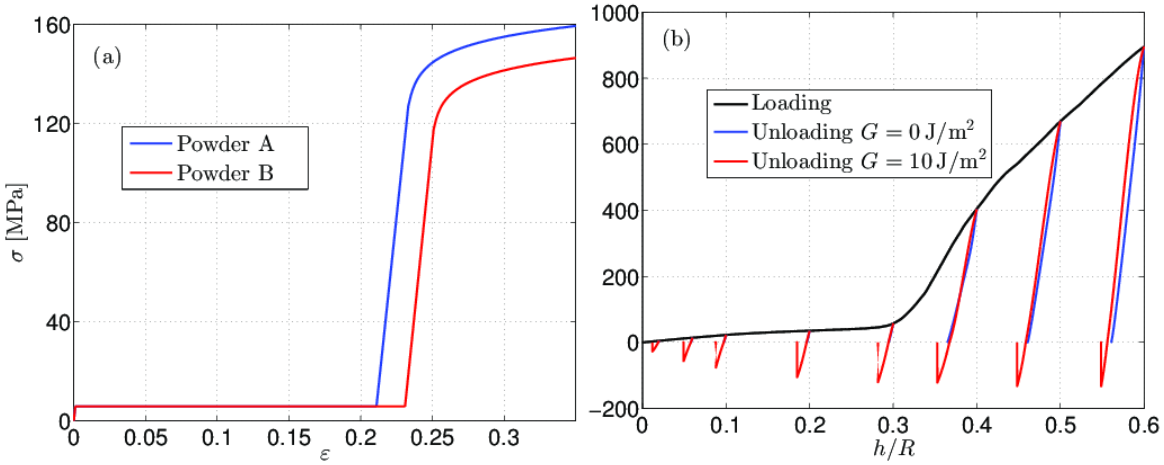

Figure 5: (a) Suggested material model for the powder granules. (b) Force-displacement relation including unloading with and without adhesion for Powder A.

5 RESULTS

The performed experiments are simulated using DEM, using the same geometry as in the experiments by having the same quotient between the diameter and height of the compacts. Previous studies [11] showed that 8000 particles is sufficient to get reliable macroscopic results.

A comparison between the experimentally determined pressure-density response and the corresponding ones from the DEM-simulations is shown in Figure 6 (a) for Powder A and 6 (b) for Powder B. The simulations agree very well with the compaction experiments for relative densities below $D < 45\%$ where the simulations start to predict a too soft response. This is due to the fact that the assumption of independent contact is not valid anymore and the contacts start to interact with each other.

The springback of the compacts are investigated by pressing the particles up to a specific relative density, with compact height L_0, and then unloading in the pressing direction until zero axial pressure, resulting in a compact height of L. Thereafter, the cylindrical wall is expanded, from radius R_0, until zero radial pressure with radius R. This method will slightly overestimate the springback in the radial direction due to the fact that the compact will shrink a little during the radial unloading. However, this small effect is neglected for simplicity.

The simulations are performed with three values on the fracture energy, $G = 0\,\mathrm{J/m^2}$, $G = 10\,\mathrm{J/m^2}$ and $G = 20\,\mathrm{J/m^2}$ but only with the material parameters determined for Powder A due to the similarity in behaviour between the different powder types.

The results show that modelling of particle bonding is essential to obtain reasonable springback values. As seen in Figure 7 (a), a much too large springback in the axial direction is predicted if bonding is not considered. Also, without bonding, the radial pressure after axial unloading is zero resulting in zero radial springback which clearly

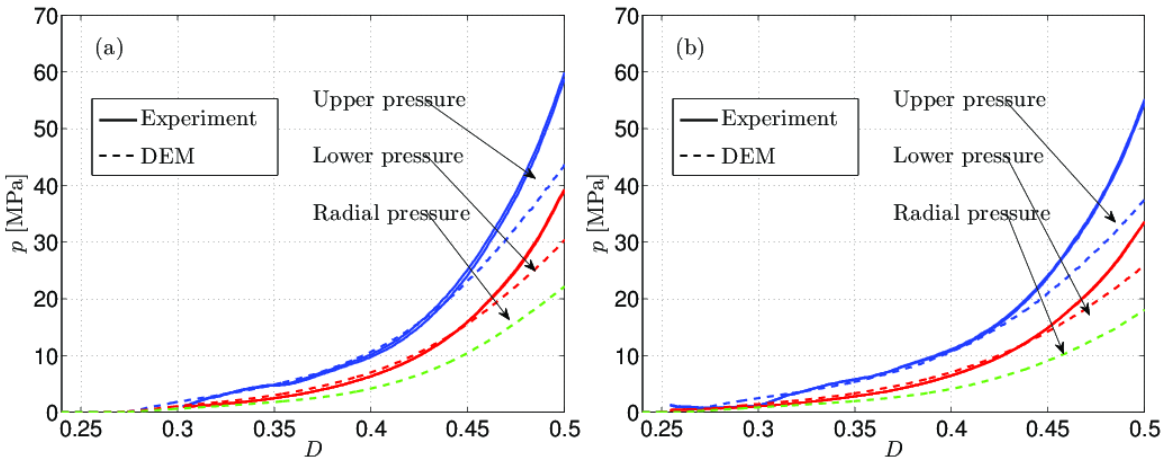

Figure 6: (a) Comparison between the DEM simulations and the results from the compaction experiments for (a) Powder A and (b) Powder B.

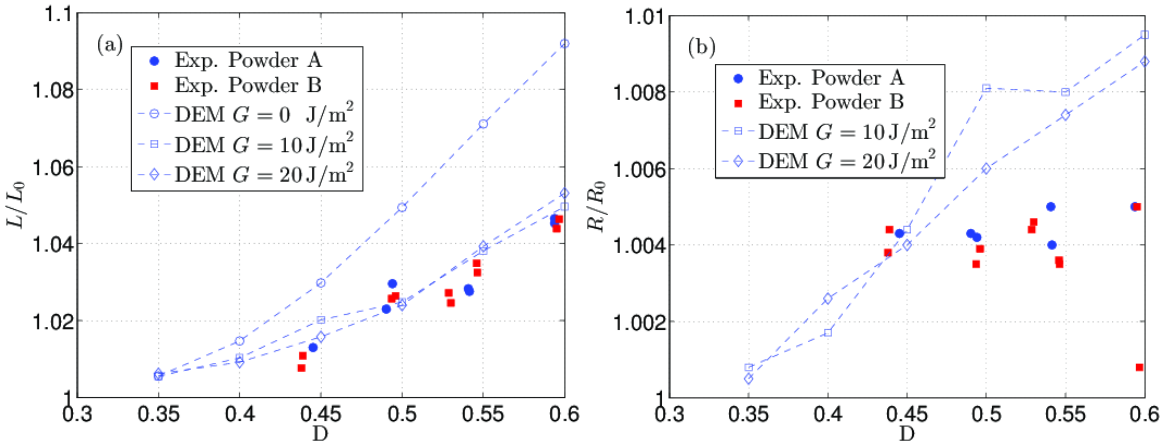

Figure 7: (a) Compairson between experimental results and DEM simulations for the springback in (a) the axial (pressing) direction and (b) in the radial direction.

does not agree with experiments. With bonding accounted for, both for $G = 10\,\mathrm{J/m^2}$ and $G = 20\,\mathrm{J/m^2}$, the simulations accurately predicts the springback in the axial direction. Interestingly, even for relative densities where the assumptions of independent contacts fails, reasonable values of the axial springback is obtained.

The numerical predictions for the radial springback, shown in Figure 7 (b) is worse. However, one should remember that these values are one magnitude lower and there are more scatter in the experimental data. Also, the diameters of the compacts were measured at one point per compact and due to the density gradient in the compact, the compacts are expected to be slightly conical after unloading.

6 CONCLUSIONS

The main results from this numerical and experimental study of powder compaction can be summarized as follows:

- Granule compaction tests together with nanoindentation tests give useful information for determining force- displacement relations pertinent to two powder particles in contact.
- The discrete element method works well for predicting the compaction behaviour up to relative densities of about 45 % corresponding to a packing density of approximately 90 %.
- The elastic modulus from nanoindentation testing, together with the fact that particle bonding is accounted for, gives good predictions on the elastic springback of powder compacts.

REFERENCES

[1] B. Storåkers, S. Biwa, P.-L. Larsson, Similarity Analysis of Inelastic Contact, Int. J. Solids. Struct. 34 (24) (1997) 3061–3083.

[2] E. Olsson, P.-L. Larsson, On Force-Displacement Relations at Contact Between Elastic-Plastic Adhesive Bodies, J. Mech. Phys. Solids 61 (5) 1185–1201.

[3] N. A. Fleck, L. T. Kuhn, R. M. McMeeking, Yielding of Metal Powder Bonded by Isolated Contacts, J. Mech. Phys. Solids 43 (9) (1992) 1139–1162.

[4] N. A. Fleck, On the Cold Compaction of Powders, J. Mech. Phys. Solids 43 (9) (1995) 1409–1431.

[5] B. Storåkers, N. A. Fleck, R. M. McMeeking, The Visco-plastic Compaction of Composite Powders, J. Mech. Phys. Solids 47 (4) (1999) 785–815.

[6] C. L. Martin, D. Bouvard, S. Shima, Study of Particle Rearrangement During Powder Compaction by the Discrete Element Method, J. Mech. Phys. Solids 51 (4) (2003) 667–693.

[7] O. Skrinjar, P.-L. Larsson, Cold Compaction of Composite Powders with Size Ratio, Acta Mater. 57 (7) (2004) 1871–1884.

[8] E. Olsson, P.-L. Larsson, On the Effect of Particle Size Distribution in Cold Powder Compaction, J. Appl. Mech. 79 (5) (2012) art. no. 050117 1–8.

[9] http://www.etewe.de/etewe-granulatfestigkeit/pruefsysteme.html.

[10] ABAQUS, Abaqus 6.11, Dassault Systèmes Simulia Corp., Providence, RI, USA (2011).

[11] E. Olsson, P.-L. Larsson, A Numerical Analysis of Cold Powder Compaction Based on Micromechanical Experiments, Powder Technol. 243 71–78.

[12] S. D. Mesarovic, N. A. Fleck, Spherical Indentation of Elastic-Plastic Solids, Proceedings of the Royal Society A 455 (1987) (1999) 2707–2728.

[13] S. D. Mesarovic, N. A. Fleck, Frictionless Indentation of Dissimilar Elstic-plastic Spheres, Int. J. Solids. Struct. 37 (46–47) (2000) 7071–7091.

[14] D. C. Andersson, P. L. Larsson, A. Cadario, P. Lindskog, On the Influence from Punch Geometry on the Stress Distribution at Powder Compaction, Powder Technol. 202 (2010) 78–88.

[15] P. Lindskog, D. C. Andersson, P. L. Larsson, An Experimental Device for Material Characterization of Powder Materials, J Test Eval 41 (3) (2012) . doi:10.1520/JTE20120107.

[16] P.-L. Larsson, Investigation of Sharp Contact at Rigid-Plastic Conditions, Int J. Mech Sci. 43 (4) (2001) 895–920.

[17] W. C. Oliver, G. M. Pharr, An Improved Technique for Determining Hardness and Elastic Modulus using Load and Displacement Sensing Experiements, Journal of Materials Research 7 (06) (1992) 1564–1583.

[18] http://www.kzkptc.com/index.htm, accessed: 19/12/2012.

[19] S. D. Mesarovic, K. L. Johnson, Adhesive Contact of Elastic-Plastic Spheres, J. Mech. Phys. Solids 48 (10) (2000) 2009–2033.

[20] C. L. Martin, Unloading of Powder Compacts and their Resulting Tensile Strength, Acta Mater. 51 (15) (2003) 4589–4602.